An Oral Vaccine Against NMDAR1 with Efficacy in Experimental Stroke and Epilepsy

Matthew J. During, *et al.*

Science **287**, 1453 (2000);
DOI: 10.1126/science.287.5457.1453

34. M. Oritz, J. Bernard, R. Personov, *Phys. Rev. Lett.* **65**, 2716 (1990).
35. W. P. Ambrose and W. E. Moerner, *Nature* **349**, 225 (1991).
36. The optical cavity is formed by two 1-mm diameter, 10-cm radius of curvature mirrors, located on the tapered end of 4 mm by 3 mm glass substrates. The multilayer dielectric mirror coatings have a transmission of 4.5×10^{-6} and absorption/scatter losses of 2.0×10^{-6}, giving rise to a cavity finesse $F = 480{,}000$. For the measured cavity length $l = 10.9$ μm and waist $w_0 = 14$ μm, we have parameters $(g_{3/2}, \kappa, \gamma) = 2\pi(110, 14.2, 2.6)$ MHz, where these rates refer to the transition $|a\rangle = |5S_{1/2}, F = 4, m_F = 4\rangle \leftrightarrow |e\rangle = |6P_{3/2}, F = 5, m_F = 5\rangle$ at $\lambda = 852$ nm in atomic cesium.
37. To interact with light in the cavity mode, an atom must fall through the 9-μm gap between the edges of the mirrors and also through the waist $w_0 = 14$ μm of the Gaussian mode of the resonator.
38. Our numerical simulations indicate that the intracavity field exhibits manifestly quantum or nonclassical characteristics for the parameters used in the experiment. For example, the normalized two-time intensity correlation function $= 0.9$ for short time delays, where a value < 1 indicates nonclassicality.
39. Experimentally, we can set a limit on atomic excursions along x by examining the amplitude of the observed oscillations. Because the oscillation frequency $\nu_x > 1.5$ MHz is well above our detection bandwidth of 100 kHz, large excursions in x would lead to substantial reductions in amplitude for the observed oscillations in transmission, from which we deduce a bound $\delta x' \approx 70$ nm for $\rho \ll w_0$. Inference of axial localization without such bandwidth limitations can be found in (*13*).
40. H. Jabaldard and C. Cohen-Tannoudji, *J. Phys. B* **18**, 1661 (1985).
41. J. P. Cordon and A. Ashkin, *Phys. Rev. A* **21**, 1606 (1980).
42. The approximations used in some of the calculations of (*23*) and also the weak driving approximation of (*24*) are not appropriate in the regime of the current work. All quantities are calculated numerically from the full quantum master equation for the internal degrees of freedom.
43. This part of the calculation was performed with a code based on Sze Tan's "Quantum Optics Toolbox," available at www.phy.auckland.ac.nz/Staff/smt/qotoolbox/download.html
44. These are technically stochastic differential equations written in their Ito form.
45. On first inspection, it might seem that the reconstruction algorithm should fail for circular orbits as well, because in the absence of large transmission oscillations the algorithm will rely on small differences between ρ'_{max} and ρ'_{min}, which are uncertain because of technical and detection noise. However, the resulting estimated angular momentum closely approximates that of a circular orbit at radius $\rho'_{max} \approx \rho'_{min}$ and is therefore the correct angular momentum for the orbit.
46. A more extensive gallery of reconstructed orbits can be viewed at www.its.caltech.edu/~qoptics/atomorbits/gallery.html.
47. V. B. Braginsky and F. Ya. Khalili, *Quantum Measurement* (Cambridge Univ. Press, Cambridge, 1992).
48. H. Mabuchi, *Phys. Rev. A* **58**, 123 (1998).
49. J. A. Dunningham, H. M. Wiseman, D. F. Walls, *Phys. Rev. A* **55**, 1398 (1997).
50. E. Betzig and R. J. Chichester, *Science* **262**, 1422 (1993).
51. X. S. Xie and J. K. Trautman, *Annu. Rev. Phys. Chem.* **49**, 441 (1998).
52. W. E. Moerner and M. Orrit, *Science* **283**, 1670 (1999).
53. S. Weiss, *Science* **283**, 1676 (1999).
54. H. Mabuchi *et al.*, in preparation.
55. H. M. Gibbs, *Optical Bistability: Controlling Light with Light* (Academic Press, Orlando, FL, 1995).

56. We gratefully acknowledge the contributions of K. Birnbaum, M. S. Chapman, H. Mabuchi, J. Ye, and S. Tan to the current research. This work is supported by the NSF, by the Office of Naval Research, by the Defense Advanced Research Projects Agency via the Quantum Information and Computation Institute administered by Army Research Office, and by Hewlett-Packard Research Labs. Work at the University of Auckland is supported by the Marsden Fund of the Royal Society of New Zealand.

25 October 1999; accepted 18 January 2000

An Oral Vaccine Against NMDAR1 with Efficacy in Experimental Stroke and Epilepsy

Matthew J. During,[1,3]* Charles W. Symes,[1] Patricia A. Lawlor,[1] John Lin,[2] Jane Dunning,[1] Helen L. Fitzsimons,[1] David Poulsen,[3] Paola Leone,[3] Ruian Xu,[1] Bridget L. Dicker,[1] Janusz Lipski,[2] Deborah Young[1]

The brain is generally considered immunoprivileged, although increasing examples of immunological responses to brain antigens, neuronal expression of major histocompatibility class I genes, and neurological autoimmunity have been recognized. An adeno-associated virus (AAV) vaccine generated autoantibodies that targeted a specific brain protein, the NR1 subunit of the *N*-methyl-D-aspartate (NMDA) receptor. After peroral administration of the AAV vaccine, transgene expression persisted for at least 5 months and was associated with a robust humoral response in the absence of a significant cell-mediated response. This single-dose vaccine was associated with strong anti-epileptic and neuroprotective activity in rats for both a kainate-induced seizure model and also a middle cerebral artery occlusion stroke model at 1 to 5 months following vaccination. Thus, a vaccination strategy targeting brain proteins is feasible and may have therapeutic potential for neurological disorders.

In the central nervous system (CNS), both the NMDA and non-NMDA subclasses of glutamate receptors are mediators of glutamatergic excitatory neurotransmission. NMDA receptors are of major interest, as they are involved in many processes necessary for brain development including neuronal migration (*1*), patterning of afferent termination (*2*), and several forms of long-term synaptic plasticity (*3*). Properties of the receptor include calcium permeability, voltage-dependent Mg^{2+} block, and slow channel kinetics (*4*). Molecular cloning has revealed three receptor subunit families (NR1, NR2, and NR3A) which form hetero-oligomeric complexes in native NMDA receptor channels (*5, 6*). NR1 subunits are essential for the formation of functional NMDA receptors, whereas addition of other subunits modifies receptor properties (*6, 7*). In addition to the role of NMDA receptors in brain plasticity and development, they have also been implicated as a mediator of neuronal injury associated with many neurological disorders including stroke, epilepsy, brain trauma, dementia, and neurodegenerative disorders (*8*).

Because of their central involvement in the cascade leading to neuronal death following a variety of cerebral insults, pharmacological NMDA receptor antagonists have been evaluated for potential clinical use. These drugs are effective in many experimental animal models of disease, and some of these compounds have moved into clinical trials (*9*). However, the initial enthusiasm for this approach has waned, because the therapeutic ratio for most NMDA antagonists is poor, with significant adverse effects at clinically effective doses, thus limiting their utility (*9*).

As an alternative approach to antagonize NMDA receptors, we investigated the hypothesis that a humoral autoimmune response targeting the NR1 subunit of NMDA receptor might have neuroprotective activity. Moreover, we also hypothesized that such autoantibodies would have minimal penetration into the CNS under basal conditions and thereby avoid the toxicity associated with traditional approaches, but following a cerebral insult, would pass into the brain more efficiently, antagonize the receptor, and thereby attenuate NMDA receptor–mediated injury.

Oral genetic vaccination with recombinant AAV. We used an oral genetic vaccine

[1]Department of Molecular Medicine and [2]Department of Physiology, University of Auckland School of Medicine, Auckland, New Zealand. [3]Department of Neurosurgery, Jefferson Medical College and Thomas Jefferson University, Philadelphia, PA 19107, USA.

*To whom correspondence should be addressed. E-mail: matthew.during@mail.tju.edu

approach for immunization. Oral vaccines are scavenged by intestinal M cells, rapidly taken up by the antigen-presenting cells (APCs) in Peyer's patches and the lamina propria, and can induce strong humoral immune responses (*10*). We recently reported a highly efficient method to transduce gut lamina propria cells by means of a recombinant AAV vector (*11*), indicating its potential use as a systemic oral vaccine also applicable to CNS disorders. A mouse NMDAR1 cDNA was subcloned into an AAV plasmid and subsequently packaged and purified (*11*) to yield a high-titer recombinant AAV virus, AAVNMDAR1 (*12*) (Fig. 1, A and C). This vector (10^9 infectious units) was administered via an orogastric tube into the stomachs of a group of rats, with a control group receiving a similar dose of a recombinant AAV virus expressing β-galactosidase (AAVlac) as described (*11*). In rats treated with the oral AAVNMDAR1 vector, transduction of intestinal cells was confirmed by polymerase chain reaction (PCR) amplification of a portion of the cytomegalovirus (CMV) promoter from genomic DNA isolated from the proximal intestine (*13*). Similarly, the PCR product was also detected in AAVlac-immunized rat intestine, but not detected in DNA from the intestine of naïve rats, or in the liver, spleen, or testis of any AAVNMDAR1- or AAVlac-immunized rats (Fig. 1B). NMDAR1 protein expression in the intestine was detected by immunohistochemistry with a commercially available NMDAR1 primary antibody and fluorescent secondary antibody at 1 month (Fig. 1D) and 5 months (Fig. 1F) after peroral dosing. Upon confocal microscopy imaging, expression was observed to be primarily in the lamina propria as previously described for AAVlac-treated animals (*11*). A total of 9×10^6 to 12×10^6 lamina propria cells were transduced at 4 weeks after immunization, with approximately $\sim 10^7$ immunoreactive cells remaining at 5 months as previously reported when *Escherichia coli* lacZ was used as the transgene (*11*). Transduced cells were immunoreactive when the antibodies MRC OX-41 and OX-62 were used to define signal regulatory proteins expressed on cells of myeloid origin (SIRP) and dendritic cells, respectively (Fig. 2).

Blood was taken and the serum analyzed for presence of specific antibodies. In AAVlac-treated animals, immunoglobulin G (IgG) antibodies were detected at 4 weeks, with titers further increasing at 16 weeks (*14*). When a purified β-galactosidase enzyme preparation was used, a commercial monoclonal antibody recognized two protein species with molecular weights of 116 and 85 kD on immunoblots (Fig. 3A). Some animals had antibodies that bound preferentially to the 85-kD species, whereas other animals had serum antibodies with higher affinity to the 116-kD protein (Fig. 3A). Immunoblotting of AAVNMDAR1 serum to a hippocampal membrane extract yielded the expected 117-kD band, consistent with the size of the native NMDAR1 receptor subunit and similarly recognized by commercial antibodies (Fig. 3B) (*14*). The sera from naïve control ($n = 4$) or AAVlac-immunized ($n = 12$) animals showed no binding to the brain extract. When brain extracts were prepared under more severe denaturing conditions, there was degradation of the native receptor as shown by monoclonal antibody binding to 32- and 67-kD fragments (Fig. 3C). Individual AAVNMDAR1 rats showed different patterns of binding to some of these fragments (Fig. 3C). These data indicate that AAV can serve as an oral

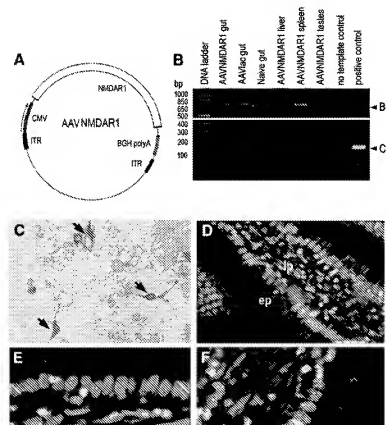

Fig. 1. Vector diagram and gut gene expression. (**A**) NMDAR1 plasmid construct and (**B**) PCR analysis. (**C**) NMDAR1 immunocytochemistry of HEK 293 cells (arrows). (**D** through **F**) NMDAR1 immunohistochemistry (blue; 1:250 dilution, Chemicon) with propidium iodide counterstaining (orange) using methods as described (*11*) to show the lamina propria (lp) and epithelial (ep) cell layers at (**D**) 4 weeks and (**F**) 5 months after AAVNMDAR1 and (**E**) 4 weeks after AAVlac administration. Scale bar: (D), 53 μm; (E) and (F), 25 μm.

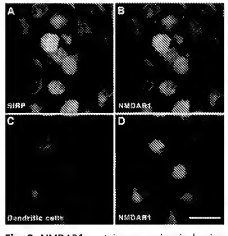

Fig. 2. NMDAR1 protein expression in lamina propria. Double immunofluorescent labeling (*19*) using monoclonal antibodies to NMDAR1 [red in (**B**), blue in (**D**)], and (**A**) SIRP (blue, 1:50 dilution, Chemicon) and (**C**) dendritic cells (red, 1:5, Chemicon). Sections were incubated with unlabeled secondary anti-mouse IgG (1:250) between primary antibody incubation steps. Primary antibodies were detected with Cy3- or Cy5-conjugated anti-mouse antibodies (1:250, Jackson Immunoresearch), and immediately prior to confocal imaging (*19*), sections were counterstained with acridine orange [green, 0.01% in PBS (pH 6.2) for 1 min], washed in PBS, and mounted in Vectashield (Vector). Bar, 10 μm.

vaccine and that immunized animals generated antibodies against a range of NMDAR1 epitopes.

Epitope mapping. To further define the range of epitopes, 94 overlapping 16–amino acid oligomers (16-mers) were synthesized that covered the entire 938 amino acids of the native NMDAR1 protein (*15*). Serum from AAVNMDAR1, AAVlac, and naïve rats was screened against this panel of 16-mers. None of the naïve ($n = 4$) or AAVlac ($n = 14$) serum screened had specific binding to any of the peptides. In contrast, AAVNMDAR1-immunized rat serum showed specific binding to peptides that corresponded to functional domains within the extracellular segments of the receptor (Fig. 3). These included peptide 49 (amino acids 483 through 498), which represents the NH_2-terminal side of M1, the first transmembrane domain (rat N19, Fig. 3E), and two peptides corresponding to the extracellular domain between M3 and M4, peptide 69 (amino acids 681 through 696; rat N21, Fig. 3F) and peptide 72 (amino acids 711 through 726; rat N64, Fig. 3H). Each of these three peptides contain critical residues for glycine binding (*16*). The most common pattern observed in serum from 7 of the 19 AAVNMDAR1 rats screened was specific binding to peptides adjacent to the M4n region (peptide 80, amino acids 791 through 807) and/or peptide 65 (amino acids 641 through 657), corresponding to the M3c domain (rat N11, Fig. 3D). Two additional rats had antibodies that bound to peptides 54 and 55 (amino acids 541 through 566; rat N52, Fig. 3G), which map to the preM1 domain. The preM1, M4n, and M3c regions form part of the extracellular vestibule of the NMDA receptor channel, where amino acid substitutions at key residues have a significant influence on channel permeability (*17*).

Cell-mediated immunity. A splenocyte proliferation assay was performed to evaluate a cell-mediated immune component associated with the vaccine. No difference in proliferative response was found between splenocytes isolated from AAVlac and AAVNMDAR1 animals challenged with the appropriate antigen (Table 1) (*18*). In addition, immunohistochemistry with $CD8^+$ and major histocompatibility complex (MHC) class I antibody markers on hippocampal sections from naïve, AAVlac, and AAVNMDAR1 rats showed no difference in $CD8^+$ or MHC class I immunoreactivity (Table 1).

Experimental epilepsy. We used the kainate model of temporal lobe epilepsy (*19*) to determine potential anti-epileptic and neuroprotective efficacy of AAVNMDAR1 vaccination. Animals received AAVNMDAR1 ($n = 9$) or AAVlac ($n = 8$), and a group of naïve control rats received no vector ($n = 17$). At 1 month following vaccination, animals were administered kainic acid (10 mg/kg body weight) intraperitoneally (i.p.), and a blinded observer determined over 2 hours whether there were any signs of the characteristic progression through various behavioral seizure stages, including immobility and staring, "wet-dog-shakes," unilateral and bilateral forelimb clonus, and facial clonus (*19*). Electroencephalographic (EEG) recordings (Fig. 4A) showed the first signs of electrographic seizure activity within 10 min after drug administration in control animals, with 13 of 17 naïve and six of the eight AAVlac animals developing facial and forearm clonus and proceeding to status epilepticus (SE). In contrast, only two of the nine AAVNMDAR1-vaccinated animals developed seizures and SE (Table 2). The remaining seven AAVNMDAR1 rats showed neither EEG changes nor any behavioral changes after kainate treatment ($P = 0.007$, chi square analysis with expected SE frequency of 68% reduced to 22% in the NMDAR1-immunized group).

To confirm that the AAVNMDAR1 vaccination was able to suppress kainate-induced seizures, we examined the hippocampi of all animals for any signs of seizure-induced neuropathology. Three days after kainate treatment, animals were euthanized before brains were removed and frozen. Coronal hippocampal sections were prepared for immunohistochemistry. No discernible TUNEL signal or clusterin immunofluorescence [a cell death marker (*20*)] was observed in the hippocampus of any animal (AAVlac, naïve, or AAVNMDAR1) that did not develop SE (Fig. 4, D and E). In comparison, all AAVlac and naïve animals that experienced SE had numerous TUNEL-positive and clusterin-immunofluorescent neurons in hippocampal CA1, CA3, and hilar regions (Fig. 4, B and C). Of the two AAVNMDAR1 animals that

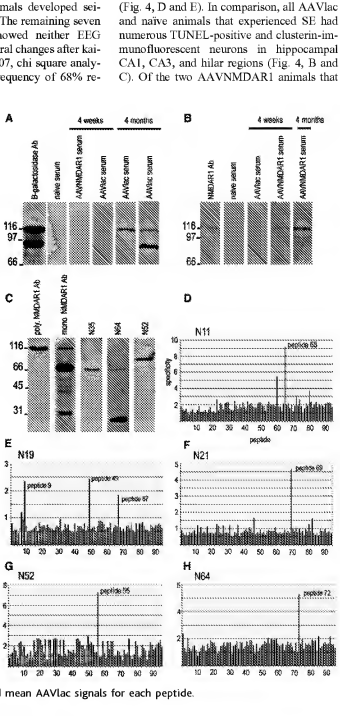

Fig. 3. Immunoblot analysis of AAVlac and AAVNMDAR1 serum and AAVNMDAR1 serum epitope mapping. **(A)** Purified β-galactosidase (1 μg per lane) was separated on a 10% acrylamide gel under reducing conditions and screened with monoclonal β-galactosidase antibody (1:5,000, Gibco BRL) and naïve, AAVlac, and AAVNMDAR1 serum (1:200) using standard immunoblot methods (*74*). **(B)** Polyclonal NMDAR1 antibody (1:250, Chemicon) and serum (1:200) from the three groups were screened against 20 μg of hippocampal extract for the presence of NMDAR1 antibodies. **(C)** Polyclonal (1:250) and monoclonal (1:3000, Chemicon) NMDAR1 antibodies and sera (1:200) were screened against 20 μg of denatured hippocampal extract. N35, N64, and N52 represent serum from three AAVNMDAR1 animals showing specific affinities for different NMDAR1 breakdown products. **(D through H)** Epitope map profiles of five (rats N11, N19, N21, N52, N64) AAVNMDAR1-treated animals. Specificity is measured as a ratio between the AAVNMDAR1 signal and mean AAVlac signals for each peptide.

Table 1. Splenocytes isolated from vaccinated rats were incubated with antigen [Hippocampal extract, recombinant NH_2-terminal NMDAR1 (N-term.), and recombinant COOH-terminal NMDAR1 (C-term.)], positive (Concavalin A) and negative (RPMI) controls with proliferation quantitated using thymidine incorporation (*18*). ND, not done. NC, not changed from negative control. MHC I (1:100, Pharmingen) and $CD8^+$ (1:200, Chemicon) immunohistochemistry was carried out (*19*) and sections were scored by densitometry and cell counting. (−), no immunoreactive cells. Cellular infiltration into the hippocampus, cortex and striatum was determined by HE staining. Neg., no inflammatory cells.

Rats	Splenocyte proliferation assay			Immunohistochemistry		Cellular infiltration
	Hippocampal extract	N-term.	C-term.	MHC I	$CD8^+$	
Naïve	ND	ND	ND	–	–	Neg.
AAVlac	NC	NC	NC	–	–	Neg.
AAVNMDAR1	NC	NC	NC	–	–	Neg.

had SE, only one of these animals (rat N12) had some injury (Fig. 4, F and G), whereas the second animal (N7) had no injury whatsoever, despite more than 45 min of severe SE (Fig. 4, H and I; Table 2). N12, the only rat to have SE as well as brain injury following AAVNMDAR1 oral dosing, was also the only animal of the nine in this experiment that did not have detectable circulating antibodies to the NMDAR1 receptor subunit. Because seizure duration is a critical determinant of the extent of neuronal injury, with as little as 30 min duration being sufficient to cause cell death (*21*), these results suggest that the AAVNMDAR1 vaccination can not only produce resistance to seizures but also protect against excitotoxic injury.

We were interested in determining if the anti-epileptic and neuroprotective effect of the NMDAR1 vaccination was nonspecific and could be reproduced with immunization against any brain protein. Therefore, we generated an AAV vector expressing GAD-65 and perorally administered this vector to an additional group of rats. These rats all developed significant antibody titers to the native protein (Fig. 5A). At 1 month following vaccination, these rats were challenged with kainate as above (*19*). All of these rats ($n = 6$) rapidly progressed to motor seizures and SE (Table 2). Analysis of their brains showed extensive damage (*22*).

To confirm passage of NMDAR1 antibodies into the brain, after 4 weeks, a group of vaccinated rats ($n = 4$) underwent nontraumatic sampling of cerebrospinal fluid (CSF) from the cisterna magna (*23*). Using immunoblot analysis and a highly sensitive chemiluminescent detection method, we were able to detect NMDAR1 autoantibodies at low levels in the CSF by immunoblotting, suggesting autoantibody passage into the brain (Fig. 5A). NMDAR1 autoantibodies were not detected in CSF from naïve ($n = 4$) or AAV-lac-immunized ($n = 4$) rats. After kainate treatment, an approximate tenfold increase in CSF levels of NMDAR1 autoantibodies was observed (Fig. 5A). In addition, IgG immunoreactivity (*24*) was specifically increased in the hippocampus in the CA3 and dentate hilar neurons, which are also susceptible to

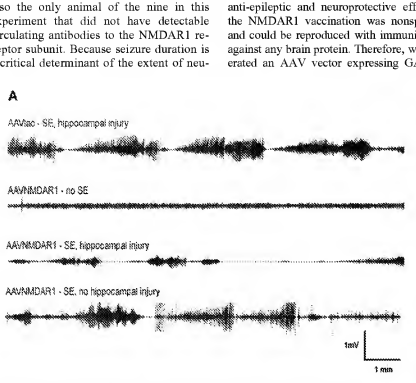

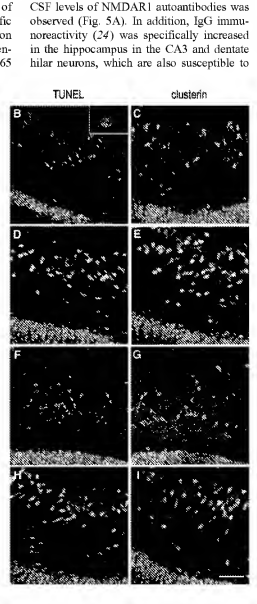

Fig. 4. Kainate-induced seizure damage in the hippocampus. (**A**) EEG recordings and (**B** through **I**) analysis of hippocampal damage in the hilus using (B, D, F, and H) fluorescent TUNEL labeling (green) or (C, E, G, and I) clusterin immunohistochemistry (green) combined with immunohistochemistry with the neuronal marker NeuN (orange) in the corresponding brains. In those rats that exhibited SE, an anticonvulsant dose of sodium pentobarbital (30 mg/kg i.p.) was administered after 45 min of continuous SE. Animals that did not develop seizures also received pentobarbital. Inset in (B) shows a high-power image of a double-labeled TUNEL and NeuN immunofluorescent neuron. (B and C) AAVlac rat developed SE. (D and E) AAVNMDAR1 rat developed no SE. (F and G) AAVNMDAR1 rat (N12) developed SE, with hippocampal injury. (H and I) AAVNMDAR1 rat (N7) developed SE, with no hippocampal injury. TUNEL and clusterin immunohistochemistry was performed as described (*19*, *20*) on 16-μm slide-mounted sections and visualized using ExtrAvidin-FITC (Sigma) and anti-rabbit FITC (Jackson Immunoresearch), respectively, prior to NeuN (1:1000, Chemicon) immunohistochemistry and anti-mouse Cy3 detection (Jackson Immunoresearch). Clusterin (1:200) was provided by D. Christie, University of Auckland, New Zealand. Bar, 200 μm.

kainate-induced neuronal damage but were protected in NMDAR1-immunized rats (Fig. 5, B through D). Furthermore, immunohistochemistry with IgG purified from AAVNMDAR1, AAVlac, or naïve serum was conducted on hippocampal sections from naïve animals that had been perfused with phosphate-buffered saline (PBS) to remove endogenous IgG present in blood vessels. Only AAVNMDAR1-purified IgG showed selective immunoreactivity in hippocampal CA3, dentate hilar, and CA1 neurons, consistent with the pattern of expression of NMDAR1 as determined with a commercial polyclonal antibody (Fig. 5, E through J).

Experimental stroke. We used the endothelin-1 model of middle cerebral artery occlusion (MCAO) (*25*) to determine the antistroke and ischemic neuroprotection efficacy of AAVNMDAR1 vaccination. In this approach, a fine needle is used to direct stereotactic delivery of endothelin-1 into the vicinity of the middle cerebral artery (MCA), which induces vasospasm leading to complete occlusion and generation of an extensive infarct in the MCA territory (including the striatum and cortex on the injected side). The model has been used previously to test novel antistroke drugs, including the NMDA receptor antagonist MK-801 (*25, 26*). Three groups of rats [naïve (n = 10), AAVlac (n = 8), and AAVNMDAR1 (n = 10)] underwent MCAO 5 months after vaccination. At 3 days after endothelin-1 administration, rats were euthanized, the brains were removed, and the infarct volume was determined by a blinded investigator (Fig. 6) (*25*). The total infarct volume was 55.6 ± 20.2 mm^3 in naïve rats and 66.4 ± 12.4 mm^3 in the AAVlac animals, whereas in the AAVNMDAR1 rats, the infarct was reduced by ~70% to 19.6 ± 6.2 mm^3 (P = 0.002, Student's t-test) (Fig. 6H). When the cortex and striatum were analyzed independently, the protection in terms of infarct volume was 65 and 80%, respectively, compared to the AAVlac group and 69 and 74%, respectively, compared to the naïve controls (Fig. 6H).

Vaccination effects on behavior. NMDA receptor antagonists administered systemically at anti-epileptic and neuroprotective doses typically result in some impairment in motor behavior (*27*). To determine whether vaccination was associated with any changes in motor behavior, rats were tested on circular track and line-crossing mobility paradigms; these tests failed to demonstrate a difference between the groups (repeated measures ANOVA, P = 0.87 and P = 0.32, respectively) (*22*).

Discussion. The brain, retina, and testis are generally perceived as immune-privileged sites, as defined traditionally by the prolonged survival of allogeneic or xenogeneic tissue transplanted into these organs. Although we now know that this immune privilege is relative and not absolute, many foreign antigens within the CNS escape immune surveillance and certain self-antigens in the brain may not induce immune tolerance; for example, in paraneoplastic disorders (PND), circulating autoantibodies interact with neuronal antigens (*28*). It is believed that brain antigens previously sequestered from the immune system via the blood-brain barrier (BBB) are presented to a naïve immune system when ectopically expressed in cancer cells and then elicit a humoral immune response (*29*). A second immune or inflammatory process may result in compromise of the integrity of the BBB, enabling a breach of the immune privilege of the brain and passage of antibodies to the targeted neurons, resulting in the characteristic disease phenotype. If this hypothesis is correct, it should be possible to vaccinate against selected brain antigens to induce a state of autoimmunity. Our study is analagous to the clinical example of PND in which a neuronal antigen is ectopically expressed (in the gut in our study, as opposed to a cancer cell in a malignant tumor), thereby inducing autoimmunity and influencing brain function.

Recently, Schenk *et al.* reported that repeated immunization with amyloid-β attenuated Alzheimer disease-like pathology in the PDAPP mouse model, possibly mediated via antibody facilitating the clearance of plaques (*30*). Also of relevance to our experiments on stroke and epilepsy are the demonstration of autoantibodies to GluR3 and GAD-65 in Rasmussen's encephalitis (*31*) and Stiffman syndrome (*32*), respectively. The Rasmussen's

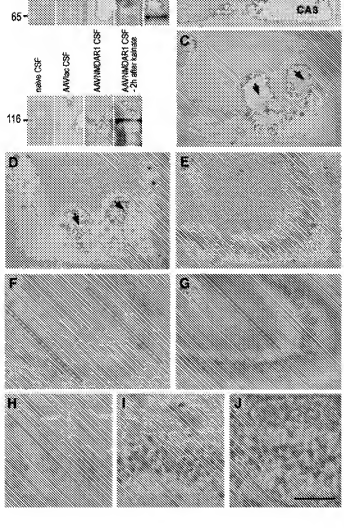

Fig. 5. Antibody passage across an intact BBB. (**A**) NMDAR1 antibody (1:5000), and naïve, AAVlac, and AAVNMDAR1 serum (1:500) was screened against 20 μg of hippocampal membrane extract, and AAVGAD65 serum (1:200) against 20 μg hippocampal cytosolic fraction by immunoblot analysis (*14*). CSF (1:5) from the same animals was screened against 30 μg of hippocampal extract for NMDAR1 antibodies. (**B** through **D**) Anti-rat IgG immunoreactivity in the hilus and CA2–CA3 region of an AAVNMDAR1-immunized rat [(B) arrows]. (C) A high-powered image of the CA3 region in (B) is compared to the same region under basal conditions [(D) arrows]. (**E** through **J**) Immunohistochemistry with 50 μg/ml (E and I) AAVNMDAR1- and (F and H) AAVlac-purified IgG, and (G and J) NMDAR1 antibody (1:250, Chemicon) and diaminobenzidine (DAB) detection (*19*) in the (E through G) CA3 and (H through J) hilar region. Scale bar: (B), 500 μm; (C through G), 200 μm; (H through J), 80 μm.

Table 2. Hippocampal injury was graded according to the extent of injury: (–), no injury; (++), moderate (<20 TUNEL or clusterin-immunofluorescent cells); (+++), extensive (>20 TUNEL or clusterin-immunofluorescent cells). Numbers in parentheses represent total number of rats in that group.

Rats	Number developing SE	Hippocampal injury in SE rats		
		(–)	(++)	(+++)
Naïve	13 (17)	–	–	13
AAVlac	6 (6)	–	–	5
AAVNMDAR1	2 (9)	1	1	–
AAVGAD-65	6 (6)	–	–	6

association was discovered when rabbits developed seizures following vaccination with a GluR3 receptor fragment. The autoantibodies were shown to have agonist properties at the receptor and thereby suggested a mechanism for hyperexcitability leading to the epilepsy associated with Rasmussen's encephalitis (*33*). Antibodies from the plasma of patients with Stiffman syndrome have been shown to bind to GAD-65 and inhibit γ-aminobutyric acid (GABA) synthesis in vitro (*34*). A GABA-deficient state may therefore lead to disinhibition and the rigidity characteristic of Stiffman syndrome. The higher than predicted (100% versus 68%) SE frequency we observed in the GAD-immunized rats supports this hypothesis.

Serum antibody titers were obtained in vaccinated animals, and we were able to detect low levels of NMDAR1 antibodies in the CSF under basal conditions. The lack of any detectable cellular immune response suggests that the likely mechanism of action of the vaccination is mediated through a humoral response consistent with the observed association between antibody titer and the neuroprotective phenotype.

NMDA receptor antagonists influence several experimental animal models of human neurological disease. The systemic administration of kainate is a well-established model of temporal lobe epilepsy. Moreover, previous studies have shown that NMDA receptor antagonism can partially inhibit seizure activity in this model in which, by activation of both pre- and postsynaptic receptors, kainate induces excessive glutamate release and NMDA-mediated neuronal excitation and injury (*35*). Our study produced a 78% anticonvulsant effect, comparing favorably with previous pharmacological studies, in which similar levels of anti-epileptic activity are typically associated with significant motor impairment (*27*).

In partial stroke models, some of the most reproducible and potent data on neuroprotection has come from the use of NMDA receptor antagonists, particularly the noncompetitive compound MK-801 (*25, 26*). However, even with this antagonist at doses that depress motor activity, tissue rescue is limited to ~50% in the cortex with no infarct reduction in the striatum (*26*). Moreover, there is a narrow time window of only a few hours in which MK-801 and other promising new antistroke drugs can be given for rescue, with effective protection requiring continued maintenance dosing (*36*).

One human study in Russia with 270 patients showed the presence of NMDA receptor autoantibodies in the serum after a stroke (*37*). Neurological recovery occurred in individuals with significant antibody titers, but poor prognosis or death was associated with the absence of NMDA receptor autoantibodies. This data further supports the clinical relevance of the vaccine.

The AAVNMDAR1-vaccinated rats generated autoantibodies, which were polyclonal. Epitope mapping of the antibodies showed a diverse range of epitopes in multiple regions of the extracellular domains. Individual animals had antibodies which bound to 16-mers that mapped to the extracellular vestibule of the channel including the preM1, M3c, and M4n domains (*16*) as well as epitopes in the NH_2-terminal region and within the extracellular loop lying between M3 and M4, which directly mapped to glycine-binding sites (*16*). Several animals did not appear to have an immunodominant epitope using the set of overlapping 16-mers, a result consistent with antibodies that are dependent on the conformational state of the protein. Further analysis of epitopes and protein fragments and correlation with neuroprotection will be necessary to define which sites of the NMDAR1 protein are the best targets for neuronal protection and vaccine development.

A major limitation of the successful translation of promising NMDA receptor antagonists to the clinic has been the significant profile of CNS-adverse effects (*9*). A potential advantage of a vaccine or antibody approach to NMDA receptor antagonism is that the receptor blockade is minimal under resting physiological conditions, under which

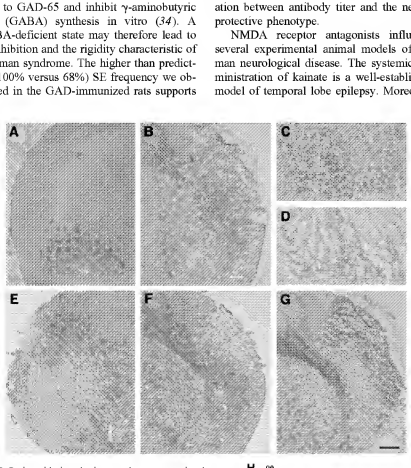

Fig. 6. Reduced ischemic damage in cortex and striatum of AAVNMDAR1-vaccinated rats after MCAO. HE staining of the striatum and/or cortical regions contralateral (**A**, **C**, and **E**) and ipsilateral (**B**, **D**, and **F**) to MCAO in (A through D) AAVlac- and (E and F) AAVNMDAR1-vaccinated animals. (**G**) Isolectin B4 (1:50, Sigma) and DAB detection (*19*) of microglial infiltration in the ipsilateral hemisphere. (**H**) Total infarct volume (mean ± SEM) in the naïve (white bars), AAVlac- (blue bars), and AAVNMDAR1-vaccinated groups (red bars). *$P < 0.01$. Scale bar: (A, B, and E through G), 600 μm; (C and D), 100 μm.

high serum titers of antibodies do not pass the BBB efficiently. However, after a neuronal insult, the BBB has increased permeability to serum antibodies, and transport and subsequent binding to the target protein can occur (*38*). This "on demand" or selective delivery of the neuroprotective agent, limited both spatially to the site of injury and to the precise timing of injury, is one of the most promising features of our approach. Of particular interest, glutamate itself has been reported to alter BBB permeability (*39*). Hence, our vaccine strategy might induce an autoprotective loop, whereby a cerebral insult increases brain extracellular glutamate and increases BBB permeability locally, resulting in facilitated passage of the autoantibody and antagonism of glutamate receptors. It has been shown that the BBB is compromised after systemic kainate administration or MCA occlusion (*40*). Whether this vaccine approach would also be effective in neurological disorders in which NMDA receptors have been implicated but the BBB remains impermeable (possibly including neurodegenerative diseases and AIDS dementia) is still unclear.

We showed neuroprotection in the rats immunized against NMDAR1 but not in the control groups including naïve, lacZ-, and GAD-65–immunized rats. Moreover, the induction of autoantibodies that bound functional domains of the NMDA receptor and that yielded a staining pattern in hippocampal slices confined to cells known to express native NR1 receptors suggests that the immunization effect was specific to the NMDA receptor. Despite this binding specificity, it remains possible that effects unrelated to receptor antagonism (for instance, antibody-mediated up-regulation of neuroprotective genes) contributed in part to the dramatic neuroprotective phenotype we observed. Furthermore, the passage into the CNS of antibodies binding to other neuronal surface proteins might also protect against neurotoxic insults and stroke. However, the epileptogenic phenotype of our GAD-65–immunized rats, all of whom progressed to SE following kainate administration, as well as previous data showing seizures in rabbits immunized against GluR3 (*31*), make a nonspecific vaccination effect less likely.

In contrast to the motor impairment associated with systemic administration of most pharmacological NMDA receptor blockers, the AAVNMDAR1-vaccinated rats had no impairment in locomotor function. Our results therefore suggest the possibility of vaccination for individuals at risk of stroke and other cerebral insults without impairment of neurological function. In support of this idea, we have collected preliminary data suggesting that far from impairing cognition, the action of the autoantibodies may parallel those of partial NMDA receptor agonists and facilitate learning and memory (*41*). Oral recombinant AAV immunization is associated with a humoral response persisting over many months and possibly years. One possible limitation is that the chronic elevation of these autoantibodies may eventually have untoward effects on brain function. We are continuing to look at long-term effects of the immunization on more complex behaviors mediated by NMDA receptors. These experiments and additional safety studies need to be investigated before any translation of this technology to the clinic.

The clinical utility of current antistroke drugs has been limited by a narrow therapeutic time window for rescue and clinical benefit. A stroke vaccine that generates autoantibodies whose access to the brain and neuroprotective activity is spatially and temporally regulated may hold promise as a prophylactic measure to protect the brain. Moreover, the ability of systemic immunization to generate autoantibodies which bind to, and thereby alter, the function of native brain proteins opens up a new avenue for modulating the nervous system and treating neurological and psychiatric disorders.

References and Notes

1. H. Komuro and P. Rakic, *Science* **260**, 95 (1993).
2. M. F. Bear, A. Kleinschmidt, Q. A. Gu, W. Singer, *J. Neurosci.* **10**, 909 (1990).
3. T. V. P. Bliss and G. L. Collingridge, *Nature* **361**, 31 (1993).
4. C. J. McBain and M. L. Mayer, *Physiol. Rev.* **74**, 723 (1994).
5. M. Hollmann and S. Heinemann, *Annu. Rev. Neurosci.* **17**, 31 (1994).
6. S. Das *et al.*, *Nature* **393**, 377 (1998).
7. M. Sheng, J. Cummings, L. A. Roldan, Y. N. Jan, L. Y. Jan, *Nature* **368**, 144 (1994).
8. M. F. Beal, *Curr. Opin. Neurobiol.* **2**, 657 (1992).
9. R. S. Schehr, *Nature Biotechnol.* **14**, 1549 (1996).
10. W. S. Shalaby, *Clin. Immunol. Immunopathol.* **74**, 127 (1995).
11. M. J. During *et al.*, *Nature Med.* **4**, 1131 (1998).
12. A full-length mouse NMDAR1 cDNA was subcloned into the AAV plasmid from the parent plasmid pSub201, under the control of a CMV immediate-early promoter and bovine growth hormone (bGH) polyadenylation site between the AAV inverted terminal repeats. Recombinant AAVNMDAR1 virus was generated helper-free as described (*11*).
13. Eight months after vector administration, genomic DNA was extracted from gut, testes, spleen, and liver by standard methods. A 141–base pair (bp) product was amplified with DNA (200 ng), CMV primers (400 nmol), CMV-1 (5′ CCCAGTACATGACCTTATGGG 3′), and CMV-2 (5′ GGAGACTTGGAAATCCCCGT 3′). Analysis of β-actin genomic DNA was used to monitor DNA integrity, using primers β-A1 (5′ CTCTTC-CAGCCTTCCTTCC 3′) and β-A2 (5′ GTCACCTTCAC-CGTTCCAG 3′) to amplify a 772-bp band.
14. Serum and antibodies were applied to nitrocellulose membranes for 1 hour at room temperature (RT) or overnight (O/N) at 4°C following a 90-min incubation in 0.1% Tween 20 containing 5% fetal bovine serum (FBS) in Tris-buffered saline. Antibodies were visualized by incubation for 1 hour at RT with peroxidase-conjugated anti-rat or anti-mouse antibody (1:12,000, Sigma) and ECL detection (Amersham). Hippocampal and cortical extracts were prepared from naïve rat brain. Two preparations were used: (i) a crude hippocampal extract was prepared by homogenization in cold 320 mM sucrose in 10 mM Tris-HCl (pH 7.4); (ii) a nondenatured membrane extract was prepared similarly but in the presence of protease inhibitors (Mini Complete, Boehringer Mannheim). After centrifugation at 7000*g* for 10 min at 4°C, the resulting supernatant was centrifuged at 37,000*g*, for 40 min at 4°C and the pellet was resuspended in 10 mM Tris-HCl (pH 7.4) containing protease inhibitors. For serum and corresponding CSF antibody screening, extracts were separated and transferred to polyvinylidene difluoride membrane, and the ECL plus (Amersham) detection system was used.
15. Ninety-six-well plates were coated with streptavidin (5 μg/ml at 37°C, O/N) followed by a 2-hour incubation with 1% FBS in 0.1% Tween 20 in PBS (PBST). Each peptide (1.2 μmol reconstituted in 0.2 ml dimethyl sulfoxide; Chiron Technologies, Clayton, Victoria, Australia) was diluted (1:1000 in PBST) before addition to the plates and incubation for 2 hours at RT. AAVNMDAR1, AAVlac, and naïve serum (1:200) were added and incubated at 4°C, O/N. Following a 1-hour incubation with peroxidase-conjugated anti-rat secondary antibody (1:40,000, RT), OPD substrate (Sigma) was applied and absorption at 490 nm was determined.
16. A. Kuryatov, B. Laube, H. Betz, J. Kuhse, *Neuron* **12**, 1291 (1994); K. A. Wafford *et al.*, *Mol. Pharmacol.* **47**, 374 (1995); M. W. Wood, H. M. VanDongen, A. M. VanDongen, *J. Biol. Chem.* **272**, 3532 (1997).
17. C. Beck, L. P. Wollmuth, P. H. Seeburg, B. Sakmann, T. Kuner, *Neuron* **22**, 559 (1999).
18. Spleens were dissected immediately upon sacrifice into complete RPMI (RPMI supplemented with 10% FBS). A cell suspension was obtained by tissue trituration and lymphocytes were cultured at a density of 6×10^5 cells/cm^2. Lymphocytes were cultured in the presence of either 50 μl antigen (protein concentration ~ 10 μg/ml), concanavalin A (5 μg/ml, Sigma), or complete RPMI. On day three, lymphocytes were incubated for 16 hours with 1.25 μCi [^{3}H]thymidine before harvesting onto filter mats and determination of thymidine incorporation.
19. D. Young, P. A. Lawlor, P. Leone, M. Dragunow, M. J. During, *Nature Med.* **5**, 448 (1999).
20. M. Dragunov et al., *Mol. Brain Res.* **32**, 279 (1995).
21. E. W. Lothman and E. H. Bertram, *Epilepsia* **34**, 559 (1993).
22. M. J. During *et al.*, data not shown.
23. Animals were anesthetized with 60 mg/kg i.p. pentobarbital, and CSF (80 to 100 μl) was drawn from the cisterna magna using a 27-gauge needle. Rats were then left at least 7 days before kainate injection (10 mg/kg i.p) and CSF sampling under anesthesia 2 hours later.
24. Naïve ($n = 4$), AAVlac ($n = 4$), AAVNMDAR1 ($n = 4$), and AAVNMDAR1 animals 2 hours after kainate administration ($n = 2$) were anesthetized before perfusion with 120 ml PBS. Anti-rat IgG immunohistochemistry (1:250, Sigma) was conducted on 16-μm hippocampal sections.
25. Endothelin-1 (60 pmol in 3 μl saline; Novablochem) was injected via a 30-gauge cannula above the MCA (AP −0.2 mm, ML 5.9 mm, DV from dura 7.5 mm) of anesthetized animals [J. Sharkey and S. P. Butcher, *J. Neurosci. Methods* **60**, 125 (1995)]. Coronal brain sections (20 μm) were taken for hematoxylin-eosin (HE) staining and isolectin B4 analysis. Infarct volume estimates were determined on serial HE sections using the Cavalieri method [H. Gundersen *et al.*, *APMIS* **96**, 857 (1988)].
26. S. P. Butcher, D. C. Henshall, Y. Teramura, K. Iwasaki, J. Sharkey, *J. Neurosci.* **17**, 6939 (1997).
27. M. Carlsson and A. Svensson, *Life Sci.* **47**, 1729 (1990); D. F. Wozniak, J. W. Olney, L. Kettinger, M. Price, J. P. Miller, *Psychopharmacology* **101**, 47 (1990).
28. J. B. Posner and H. M. Furneaux, in *Immunologic Mechanisms in Neurologic and Psychiatric Disease*, B. H. Waksman, Ed. (Raven Press, New York, 1990), pp. 187–219.
29. R. B. Darnell, *Proc. Natl. Acad. Sci. U.S.A.* **93**, 4529 (1996).
30. D. Schenk *et al.*, *Nature* **400**, 173 (1999).
31. S. W. Rogers *et al.*, *Science* **265**, 648 (1994).
32. M. Solimena *et al.*, *N. Engl. J. Med.* **318**, 1012 (1988).

33. R. E. Twyman, L. C. Gahring, J. Spiess, S. W. Rogers, *Neuron* **14**, 755 (1995).
34. K. Dinkel, H. M. Meinck, K. M. Jury, W. Karges, W. Richter, *Ann. Neurol.* **44**, 194 (1998).
35. H. Baran, W. Loscher, M. Mevissen, *Brain Res.* **652**, 195 (1994).
36. G. K. Steinberg *et al.*, *Neuroscience* **64**, 99 (1995).
37. E. I. Gusev, V. I. Skvortsova, G. A. Izykenova, A. A. Alekseev, S. A. Dambinova, *Zh. Nevropatol. Psikhiatr. Im. S. S. Korsakova* **96**, 68 (1996).
38. N. Aihara, H. Tanno, J. J. Hall, L. H. Pitts, L. J. Noble, *J. Comp. Neurol.* **342**, 481 (1994).
39. W. G. Mayhan and S. P. Didion, *Stroke* **27**, 965 (1996).
40. D. K. Zucker, G. F. Wooten, E. W. Lothman, *Exp. Neurol.* **79**, 422 (1983); S. Albayrak, Q. Zhao, B. K. Siesjo, M. L. Smith, *Acta Neuropathol.* **94**, 158 (1997).
41. M. J. During *et al.*, in preparation.
42. We thank D. Wu, P. Schweder, J. Francis, S. McPhee, and R. Bland for general technical assistance and advice, C. G. Janson, J. Heywood, M. Dragunow, J. Fraser, and K. Lehnert for scientific assistance, helpful discussions, and manuscript review, T. Hughes for the NMDAR1 cDNA, and X. Xiao and R. J. Samulski for the original AAV cloning and packaging plasmids and advice regarding generation of recombinant AAV vectors. Supported in part by the New Zealand Marsden Fund, New Zealand Health Research Council, and the Jefferson Faculty Foundation.

4 November 1999; accepted 21 January 2000

REPORTS

Shaped Ceramics with Tunable Magnetic Properties from Metal-Containing Polymers

Mark J. MacLachlan,[1] Madlen Ginzburg,[1] Neil Coombs,[1] Thomas W. Coyle,[2] Nandyala P. Raju,[3] John E. Greedan,[3] Geoffrey A. Ozin,[1]* Ian Manners[1]*

A shaped, magnetic ceramic was obtained from a metal-containing polymer network, which was synthesized by thermal polymerization of a metal-containing organosilicon monomer. Pyrolysis of a cylinder, shape, or film of the metal-containing polymer precursor produced a low-density magnetic ceramic replica in high yield. The magnetic properties of the shaped ceramic could be tuned between a superparamagnetic and ferromagnetic state by controlling the pyrolysis conditions, with the particular state dependent on the size of iron nanoclusters homogeneously dispersed throughout the carbosilane-graphitic–silicon nitride matrix. These results indicate that cross-linked metal-containing polymers may be useful precursors to ceramic monoliths with tailorable magnetic properties.

High-performance ceramics, such as SiC, AlN, B_4C, and TiN, are of widespread technological importance in applications as diverse as rocket nozzles and automobile parts (*1–3*). Ceramics obtained as films, coatings, fibers, or bulk shapes are especially appealing for practical applications. Ceramic materials are generally prepared from powders in a sequence of synthesis, processing, shaping, and sintering steps. Recent studies suggest that organosilicon polymers and inorganic glasses may be more practical precursors to advanced ceramics, as they have the advantage of a three-dimensional network of covalent bonds and ease of processibility familiar to polymer and sol-gel science (*4–8*). Most work on polymer-derived ceramics has focused on the mechanical strength and stability of materials, rather than electronic and magnetic properties (*9–13*). Furthermore, the ceramic materials previously obtained from metal-containing polymers are powders. Shaped ceramics with tunable magnetic properties may find utility as protective coatings, magnetic recording media, and antistatic shielding.

Although of considerable interest (*7–15*), the preparation of nonoxide ceramics from organometallic polymers has been hindered by the synthetic challenge of conveniently preparing well-characterized precursor materials with appreciable molecular weights. The ring-opening polymerization (ROP) of strained [1]silaferrocenophanes (SFP, Fig. 1A) is a well-established route to high–molecular weight poly(ferrocenylsilanes) (PFS, Fig. 1B) (*16–18*). Upon pyrolysis at 1000°C under N_2, PFS yields a magnetic ceramic powder but in low yield (30 to 40%) (*19*). The resulting powders contain ferromagnetic iron particles within the SiC-C-Si_3N_4 matrix. We have shown that pyrolysis of nanoscale cylinders of PFS in hexagonal mesoporous silica at 900°C yields iron nanocrystals with a diameter constrained by the width of the channels (*20*).

An important consideration when choosing a ceramic precursor is the ceramic yield because this ultimately determines the utility, bulk properties, and shape retention in the resulting ceramic. Cross-linking preceramic polymers is a prevalent method for increasing the ceramic yields because it reduces the amount of volatile decomposition products. In this regard, we chose to form an example of a cross-linked metal-containing polymer precursor to demonstrate shape retention in the resulting ceramic. This was achieved starting with the spirocyclic [1]silaferrocenophane (SSFP, Fig. 1C) (*21*, *22*).

Differential scanning calorimetry of SSFP displayed a melt at 92°C followed immediately by an exotherm with two peaks, consistent with ROP. When SSFP was heated in a sealed Pyrex polymerization tube under vacuum at 140°C for 12 hours and then at 180°C for 4 hours, it appeared to melt and rapidly became immobile. The resulting orange-red solid was stirred for 48 hours in tetrahydrofuran (THF) under N_2, but only a small amount of material dissolved. Gel permeation chromatography of the soluble fraction showed no polymer; it probably contained only residual monomer and short oligomers.

The cross-linked preceramic polymer network (CPPN) was characterized by powder x-ray diffraction (PXRD), solid-state magic-angle spinning (MAS) nuclear magnetic resonance (NMR) (^1H, ^{13}C, and ^{29}Si), thermogravimetric analysis, and pyrolysis mass spectrometry. A PXRD pattern of the CPPN displays two sharp reflections at 2θ = 12.81°, d = 6.90 Å [full width at half maximum (FWHM) intensity = 0.29° 2θ] and 2θ = 15.38°, d = 5.76 Å (FWHM = 0.41° 2θ) corresponding to diffraction coherence between iron centers in the cross-linked polymer network. (θ is the angle of incidence of the x-ray beam on the sample, and d is the lattice spacing.) Also observed are some broad halos revealing additional short-range order in the material.

^1H MAS NMR of the CPPN showed two peaks centered at 3.9 ppm and 1.8 ppm, attributed to the cyclopentadienyl (Cp) and methylene resonances, respectively. In the ^{13}C cross-polarization MAS (CP-MAS) NMR spectrum of the CPPN (Fig. 2), two resonances associated with the methylene groups of the carbosilane were observed at 18 and 26 ppm. In the Cp region, several peaks observed between 73.2 and 76 ppm are consistent with Cp (C–H) carbons. Also, three

[1]Department of Chemistry, University of Toronto, 80 St. George Street, Toronto, Ontario M5S 3H6, Canada. [2]Department of Metallurgy and Materials Science and Department of Chemical Engineering and Applied Chemistry, University of Toronto, 184 College Street, Toronto, Ontario M5S 3E4, Canada. [3]Brockhouse Institute for Materials Research, McMaster University, Hamilton, Ontario L8S 4M1, Canada.

*To whom correspondence should be addressed. E-mail: gozin@alchemy.chem.utoronto.ca; imanners@alchemy.chem.utoronto.ca